crystals

MDPI

Article

The Formation Mechanism of $Cu(In_{0.7}Ga_{0.3})Se_2$ Nanoparticles and the Densification Trajectory of the Se-Rich Quaternary Target by Hot Pressing

Qiang Ma [1,2], Weijia Zhang [1,*], Zhaoyi Jiang [1], Denghao Ma [1], Yulong Zhang [1], Chaoqun Lu [1] and Zhiqiang Fan [1]

[1] Center of Condensed Matter and Material Physics, School of Physics and Nuclear Energy Engineering, Beihang University, Beijing 100191, China; maq@nxu.edu.cn (Q.M.); jzy@163.com (Z.J.); madenghao1987@163.com (D.M.); YulongZhang@163.com (Y.Z.); luchaoqun@126.com (C.L.); fanzhiqiang@126.com (Z.F.)

[2] Institute of Ethnic Preparatory Education, Ningxia University, Yinchuan 750021, China

* Correspondence: zwjghx@buaa.edu.cn; Tel.: +86-135-2153-3929

Received: 1 March 2018; Accepted: 14 March 2018; Published: 15 March 2018

Abstract: In this paper, a method to obtain the $CuInGaSe_2$ (CIGS) absorber layer with an appropriate selenium content is put forward, in which a Se-rich target is used to deposit a CIGS thin-film and this film is annealed in a Se-free inert atmosphere. The key issue of this method is the preparation of a Se-rich target with a homogeneous composition and a high-density. The formation mechanism of $CuInSe_2$ and $CuGaSe_2$ is investigated and the results point to the intermediate phase $Cu_{2-x}Se$ playing a role of a nucleation core. The sintering densification trajectory of the target with the addition of extra selenium is researched. Additionally, an effective way to avoid the sintering defects is proposed. Finally, a conversion efficiency of 11.2% for the CIGS solar cell is reached by sputtering from the obtained Se-rich target.

Keywords: Se-rich target; hot pressing; CIGS; formation mechanism

1. Introduction

Sputtering using quaternary $CuInGaSe_2$ (CIGS) targets to deposit a thin-film of CIGS and annealing it in an atmosphere containing Se could prepare high-quality absorber layers and photovoltaic cells with high conversion efficiency [1,2]. Currently, H_2Se gas is chosen to be the selenium source; however, it is of active reactivity and highly toxic, thus requiring higher corrosion protection and gas tightness in experimental facilities [3–7].

A novel method is proposed to obtain the deposited CIGS film with more selenium than that of the stoichiometric ratio by sputtering from a Se-rich target [8,9]. The deposited CIGS film can be annealed in an inert atmosphere in a selenium-free atmosphere at a high temperature. This way, the desirable selenium content of the absorber layer can be ensured. Thus, the toxic H_2Se could be avoided, which not only simplifies the process and the experimental facilities, but also makes the film more homogeneous. Several groups have also employed such a method and fabricated high-quality devices. However, the fabrication of a Se-rich target, which is the important but difficult part of the method, are seldom researched hitherto. In this paper, a novel and effective method is utilized to prepare the Se-rich target, by incorporating additional elemental selenium into the mixed film. As is known, nanoparticles with fine and uniform size are the key issue in fabricating targets with high-density and homogeneous composition. The solvothermal method and heat injection method were used to obtain CIGS nanoparticles [10–12]. However, there exist some problems, such as the separation of the $CuInSe_2$ (CIS) phase and the $CuGaSe_2$ (CGS) phase, the composition deviation

of the raw powders from the obtained particles, and the low production efficiency. In this paper, to overcome the above-mentioned problems, high-temperature solid-phase synthesis is used to prepare the CIGS nanoparticles. The study on the CIGS formation mechanism by solid phase synthesis has not been widely investigated. Some researchers deemed that the CIS phase forms from a reaction between Cu_2Se and In_2Se_3. Afterwards, the CGS phase forms from a reaction between the Cu_2Se and Ga_2Se_3 followed with the formation of the CIGS phase by the complete inter-diffusion [13]. However, the formation mechanism of CIS and CGS still lacks in-depth research.

As the most important performance index, target density is one of the key issues we focused on. A target of low density means porous microstructure, which hinders the transport of free electrons and reduces the electrical and thermal conductivity [14,15]. Additionally, targets with low density are difficult, giving rise to a discharge of plasma, and cooling that must be used in the sputtering, which affects the usage of the target and shortens its lifespan [16]. As a result, various kinds of targets used for semiconductor films, manufactured by sputtering, are high-density targets. The high-density Se-rich target can be obtained by the hot-pressing method [17,18], however the densification trajectory is not researched explicitly enough. In this paper, these areas lacking research are analyzed thoroughly.

2. Experimental Procedure

A two-step method was employed to fabricate a Se-rich target, which included the preparation of single phase CIGS nanoparticles and the preparation of a Se-rich target, respectively. In the first step, the Cu_2Se ($\geq$99.99%), In_2Se_3 ($\geq$99.99%), and Ga_2Se_3 (gallium selenide, 5N) powders were used to prepare the CIGS nanoparticles. The molar ratio of the raw materials was designed as 0.90:0.72:0.28. To facilitate uniformity, the powders were put into a nylon jar together with zirconia balls and ethanol for ball milling by using a commercial ball grinder. Ethanol was chosen as the powders are more soluble in it than in deionized water. This way, the mixture particles are finer after milling. The ratio of the weight of the balls to the powder and the ethanol was 4:1:2. The mixed powders were milled for 2 h at a rotating speed of 400 rpm. The ball and powder mixture were dried and sieved after milling. The obtained mixture powders had a medium size less than 2 μm. Then, the mixture powders were put into the hot-pressing furnace to form a bulk of CIGS under a pressure of 3 MPa at 700–800 °C. After that, the bulk of CIGS was crushed into CIGS powder.

In the second step, with the addition of corresponding elemental selenium powder to the CIGS powders, the mixed powders were milled again for 2 h for homogenization. The molar ratio of Se and CIGS was 1:10. The milled mixture was sintered in the hot-pressing furnace with a sintering pressure of 30 MPa and a sintering atmosphere of 0.9 atm nitrogen under 580 °C for 2 h. The sizes of the targets were $\Phi 60 \times 5$ mm^3 and $120 \times 80 \times 5$ mm^3, respectively. The details are shown as follows: a pressure of 3 MPa was conducted when the sintering temperature was rising from room temperature to 200 °C. When it reached 200 °C, the temperature was kept constant for 30 min, while the pressure was raised to 30 MPa gradually. After that, the temperature was raised to 580 °C with a heating rate of 10 °C/min, while the pressure was maintained. After reaching 580 °C, the temperature and pressure were kept constant for 2 h to naturally cool.

The magnetron sputtering equipment with middle-frequency sputtering powers was applied for preparing CIGS films. The sputtering process was accomplished with a sputtering power of 0.7 W/cm^2 for 60 min in an Ar atmosphere of 0.7 Pa. The CIGS thin films were deposited on soda-lime glass with a thickness of about 1.2 μm. The following annealing process was performed in a quartz tube furnace. The annealing temperature was 525–575 °C while the annealing time was 30 min and the annealing ambient gas was N_2.

The X-ray fluorescence (XRF, LAB CENTER XRF-1800, Japan) was used to analyze the composition of the powders and target. The crystal structures were investigated using an X-ray diffractometer (XRD, Rigaku smartlab, Japan) with Cu Kα radiation. The microstructure was analyzed under a scanning electron microscope (SEM, ZEISS SIGMA, Germany). The sintered densities of the targets were determined using Archimedes' method in distilled water. The performances of the solar cells

were deduced from J-V curves of Keithley 2400 under AM 1.5 (100 mW/cm^2) illumination which was provided by a 91192-1000 solar simulator from Newport.

3. Results and Discussion

3.1. The Formation Mechanism of CIGS

The resulting powder of the first step was characterized by XRD, as shown in Figure 1. It was observed that the top three peaks were very sharp, indicating a single chalcopyrite phase. Besides these three strong peaks, there were several small peaks. These smaller peaks could be ascribed to the diffraction peaks of the CIGS phase as well.

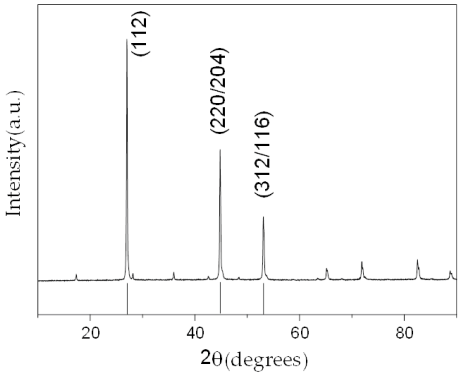

Figure 1. X-ray diffraction patterns of $CuInGaSe_2$ (CIGS) nanoparticles synthesized at 800 °C for 2 h.

The precursor composition of the mixture powders and the synthesized CIGS are shown in Table 1. The synthesized CIGS have a ratio of 0.9:0.75:0.30:1.90 (Cu:In:Ga:Se), which is close to the precursor composition.

Table 1. The chemical composition measured by X-ray fluorescence (XRF) of the $CuInGaSe_2$ (CIGS) nanoparticles prepared using the solid phase synthesis process.

Element	Cu (at)%	In (at)%	Ga (at)%	Se (at)%
Precursor Composition	23.38	18.18	7.79	50.62
Composition	23.25	19.71	7.80	49.47

It was found that these powders started to react from the milling process. The Cu_2Se and In_2Se_3 powders were milled for 1 h and the resulting phase structure is shown in Figure 2a. It was found that $Cu_{2-x}Se$ (PDF No. 06-0680), CuSe (PDF No. 20-1020), and Cu_3Se_2 (PDF No. 47-1745) appeared in addition to the presence of In_2Se_3. Similarly, the Cu_2Se and Ga_2Se_3 powders were milled for 1 h and the resulting phase structure is shown in Figure 2b. It was found that $Cu_{2-x}Se$ (06-0680), Cu_3Se_2 (47-1745), and GaSe (PDF No. 29-0628) appeared in addition to the presence of Ga_2Se_3.

Thus, it could be discovered that Cu_2Se was oxidized to Cu_3Se_2 by In_2Se_3 and Ga_2Se_3, and part of the generated Cu_3Se_2 decomposed into $Cu_{2-x}Se$ and the CuSe phase when milling. The reaction equations could be concluded from the above observation and analysis:

$$3Cu_2Se + In_2Se_3 == 2Cu_3Se_2 + 2InSe \quad (1)$$

$$3Cu_2Se + Ga_2Se_3 == 2Cu_3Se_2 + 2GaSe \quad (2)$$

$$Cu_3Se_2 == Cu_{2-x}Se + CuSe \quad (3)$$

Then, the mixture powders consisting of Cu_2Se, In_2Se_3, and Ga_2Se_3 were milled for 2 h and the phase structure of the powders was characterized by XRD patterns. As shown in Figure 3, CIS and CGS started to generate during this milling process.

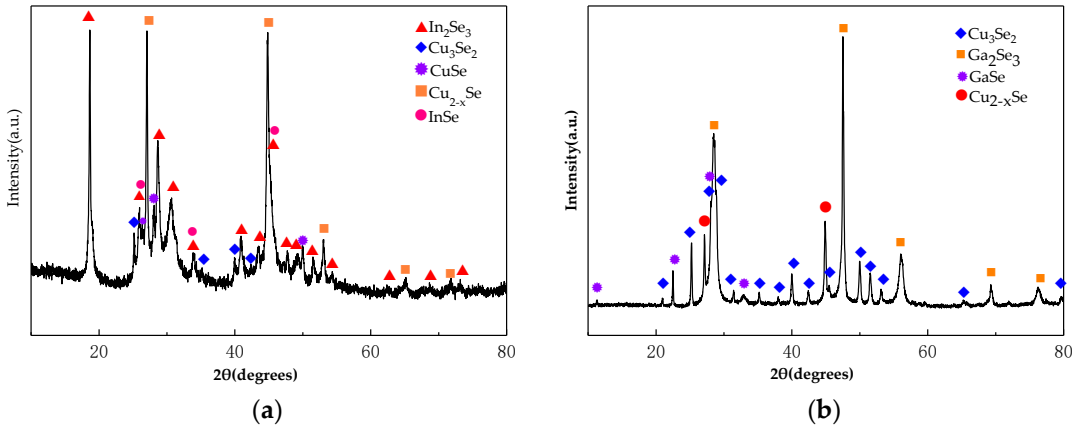

Figure 2. The X-ray diffraction patterns of the Cu_2Se and In_2Se_3 mixture powders (**a**); and the Cu_2Se and Ga_2Se_3 mixture powders (**b**) after 1 h of milling.

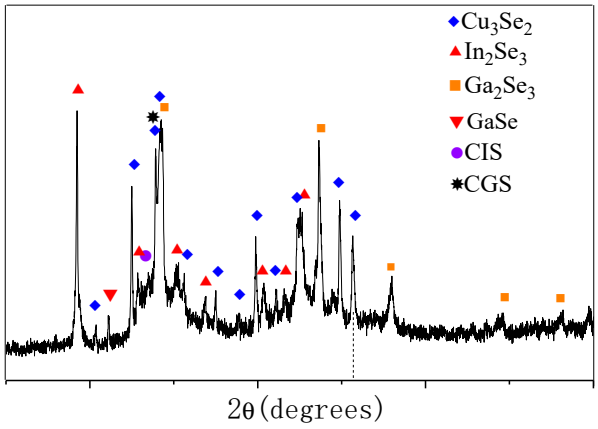

Figure 3. The X-ray diffraction patterns of the Cu_2Se, In_2Se_3, and Ga_2Se_3 mixtures milled for 2 h.

Compared with the raw material Cu_2Se, $Cu_{2-x}Se$ has a totally different crystal structure. The latter is face-center-cubic (FCC), which is similar to the chalcopyrite CIGS phase. For the $Cu_{2-x}Se$ structure, Se atoms form an FCC frame and the Cu^+ ions are highly mobile and behave in a liquid-like manner with a reduced mean free path for phonons. Presumably, with this easy-migration characteristic, the Cu^+, In^{3+}, and Ga^{3+} ions diffuse into the interior of the $Cu_{2-x}Se$ substrate to fill in the vacancies of the Cu, forming the CIS and CGS phases.

Combined with previous studies by other researchers [11,19–23], it can be suggested that the reactions be carried out as follows:

$$CuSe == Cu_{2-x}Se + Se \text{ (rich liquid when the temperature reaches 380 °C)} \quad (4)$$

$$Cu_{2-x}Se + In_2Se_3 + InSe == CuInSe_2 \quad (5)$$

$$Cu_{2-x}Se + Ga_2Se_3 + GaSe == CuGaSe_2 \quad (6)$$

$$CuInSe_2 + CuGaSe_2 == Cu(InGa)Se_2 \quad (7)$$

3.2. The Densification Trajectory of the Se-Rich Target

Figure 4 shows the curves of temperature, pressure, and pressure head displacement against time after the temperature reached 200 °C. The displacement of the pressure head revealed the process of densification, which was recorded by the grating ruler of the furnace. The density variation with time is the key research part of the sintering process. From the curve of pressure head displacement with time, the sintering process could be divided into four stages.

In the first stage, the temperature is kept constant while the pressure was raised from 3 MPa to 30 MPa for the first 30 min of sintering. The sintered compact thickness decreased linearly with the increased pressure. The powders could be regarded as perfectly elastic bodies and Hooke's law could be applied to the pressing process [24,25]. In this stage, the relative sliding of the particles, including displacement and rearrangement, occurred while the pores between particles diminished. Thus, the pressure head displacement increased linearly with time, as shown in Figure 4.

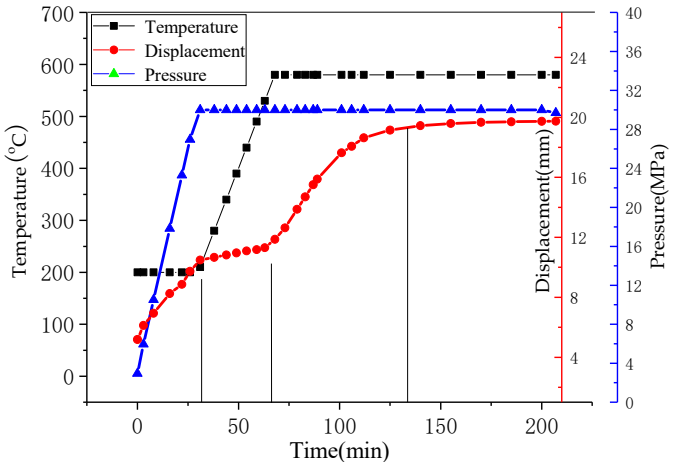

Figure 4. The variant on the curves of temperature, pressure, and pressure head displacement with time.

In the second stage, the densification rate decreased when the pressure was kept constant and the temperature increased from 200 °C to 580 °C. After the powders were pressed, the density had attained a certain value and there emerged a compression resistance for the powders. Therefore, it was difficult to further improve the density. With the increasing temperature, the particles were afforded more migration energy, thus the density of the sintered compact slightly increased.

In the third stage, heat preservation began after the temperature reached 580 °C. It was during that period that the rapid densification occurred. That is, the density of the sintered compact increased rapidly. Because, in high temperature, the effective pressure on the contact area of the particles is greater than the yield stress of the powders, the plastic flow and plastic deformation of particles occurred, which resulted in an increase to the contact area and the number of contact points between the particles. In addition, the liquid selenium weakened the occlusal force between the particles which was conducive to the material transfer to promote the densification process.

In the final stage, the density increased slowly. In Figure 5, it is found that the FWHM (full width at half maximum) decreased and the grain size increased with the sintered time. In this period, the pores between particles closed, shrunk, and disappeared gradually. The grain boundary diffusion and diffusion creep played key roles in the densification process. With the density increasing and grain growing, the average contact area increased, while the effective partial pressure generated in the particle contact area reduced, which lowered the densification rate. The densification process was completely stopped until it reached the final density. The sintered time of 2 h for the Se-rich target was appropriate as the ultimate density had been reached. There was no need to prolong the time as the oversize grain led to the delamination of the targets.

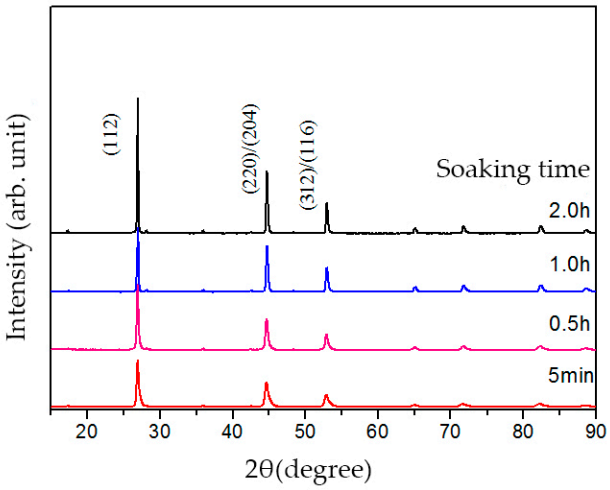

Figure 5. The crystallinity variation of sintered compact with time under 30 MPa pressure at 580 °C.

3.3. The Performance of the Se-Rich Target and Solar Cell

The composition of the mixture powders and the target are listed in Table 2. Compared with the mixture powders, there was a slight loss of the elemental selenium in the targets. The relative densities of the targets were 94.75%, 96.07%, and 95.13%, respectively, which met the requirement of sputtering. The films are obtained by sputtering the target and annealing in a protective atmosphere. The compositions of the films are listed in the table as well. Compared with the composition of the targets, the film possessed less of the group III elements. This might be ascribed to the formation of gaseous phase Ga_2Se and In_2Se.

Table 2. The composition of the mixture powder and targets.

Elements	Cu (at)%	In (at)%	Ga (at)%	Se (at)%
CIGS + Se	23.03	18.93	7.78	50.46
Target 1	23.27	18.86	7.77	50.27
Target 2	23.24	18.88	7.77	50.27
Target 3	23.23	18.82	7.77	50.35
Annealed film	23.90	18.21	7.43	50.46

The obtained CIGS thin film through sputtering from the prepared targets was annealed under 0.5 atm of N_2, and the cross-sectional microstructure of the annealed film was demonstrated in Figure 6a, which exhibits low roughness and good crystallinity. Subsequently, CdS, i-ZnO, and AZO layers were fabricated successively. The current–voltage curve is displayed in Figure 6b. The conversion efficiency was calculated to be 11.21%. Compared with the CIGS devices by both the three-stage co-evaporation and the selenization of Cu-In-Ga precursor methods, the efficiency of the devices by sputtering the Se-rich CIGS target was not desirable. However, the photovoltaic characteristics prove that the route of the Se-rich target could be an effective way of fabricating low-cost and non-toxic CIGS devices. It is believed that the performance of the solar cell could be improved more after the optimization of the process.

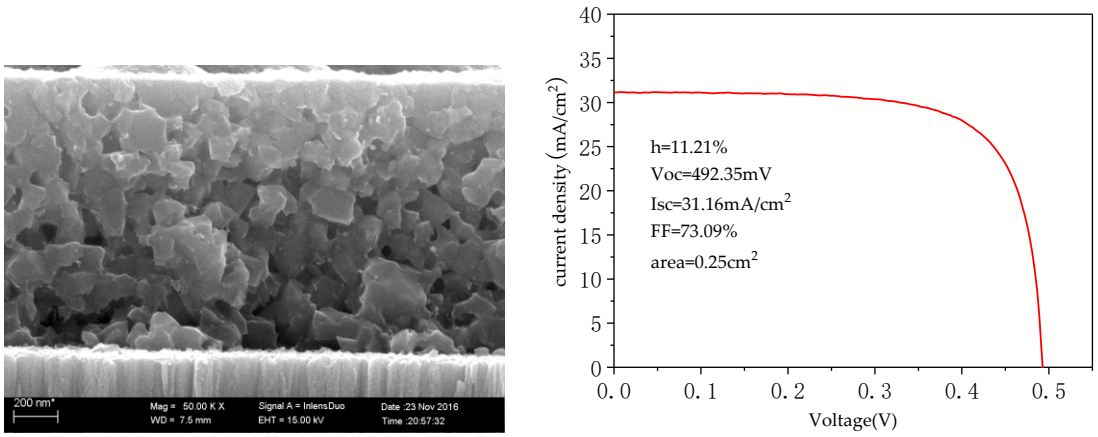

Figure 6. (**a**) The microstructure of CIGS absorber; and (**b**) the current–voltage performance curve.

4. Conclusions

The single-phase CIGS nanoparticles and Se-rich target are prepared in this study by the two-step hot-pressing method. The formation mechanism of CIGS and the densification trajectory are investigated in-depth. The phases of the milling process demonstrate that $Cu_{2-x}Se$ might be the formation core, followed by the diffusion of In and Ga atoms, and the resultant CIS phase and CGS phase. The sintering curve indicates the sintering period of the Se-rich target could be divided into four stages, regardless of the addition of liquid selenium. This research provides a clearer understanding of the formation of the CIGS phase and a more distinct comprehension of the hot-pressing sintering process.

Acknowledgments: The authors gratefully acknowledge Beihang University for providing access to the experimental equipment used for the fabrication and measurement of samples. The project as a whole is supported by the National Natural Science Foundation of China (Grant No.: 51572008).

Author Contributions: Qiang Ma and Weijia Zhang conceived and designed the experiments; Qiang Ma, Zhaoyi Jiang, Chaoqun Lu performed the experiments; Qiang Ma, Denghao Ma, Yulong Zhang, Zhiqiang Fan analyzed the data; Qiang Ma wrote the paper.

Conflicts of Interest: The authors declare no conflict of interest.

References

1. Kim, K.; Park, H.; Hanket, G.M.; Kim, W.K.; Shafarman, W.N. Composition and bandgap control in Cu(In,Ga)Se_2-based absorbers formed by reaction of metal precursors. *Prog. Photovolt. Res. Appl.* **2015**, *23*, 765–772. [CrossRef]
2. Ouyang, L.; Zhao, M.; Zhuang, D.; Han, J.; Gao, Z.; Guo, L.; Li, X.; Sun, R.; Cao, M. Annealing treatment of Cu(In,Ga)Se_2 absorbers prepared by sputtering a quaternary target for 13.5% conversion efficiency device. *Sol. Energy* **2015**, *118*, 375–383. [CrossRef]
3. Shi, J.H.; Li, Z.Q.; Zhang, D.W.; Liu, Q.Q.; Sun, Z.; Huang, S.M. Fabrication of Cu(In, Ga)Se_2 thin films by sputtering from a single quaternary chalcogenide target. *Prog. Photovolt. Res. Appl.* **2011**, *19*, 160–164. [CrossRef]
4. Stanbery, B.J. Copper indium selenides and related materials for photovoltaic devices. *Crit. Rev. Solid State* **2002**, *27*, 73–117. [CrossRef]
5. Ciccarelli, G.; Fthenakis, V.M.; Boccio, J.L. A method of analysis for gas explosions: H_2se case study. *J. Loss Prev. Process Ind.* **1999**, *12*, 157–165. [CrossRef]
6. Peng, X.; Zhao, M.; Zhuang, D.M.; Sun, R.J.; Zhang, L.; Wei, Y.W.; Lv, X.Y.; Wu, Y.X.; Ren, G.A. Fabricating Cu(In,Ga)Se_2(CIGS) thin films with large grains based on the quaternary CIGS targets. *Vacuum* **2017**, *146*, 282–286. [CrossRef]

7. Zhang, L.; Zhuang, D.; Zhao, M.; Gong, Q.; Guo, L.; Ouyang, L.; Sun, R.; Wei, Y.; Zhan, S. The effects of selenium content on Cu(InGa)Se_2 thin film solar cells by sputtering from quaternary target with se-free post annealing. *Vacuum* **2017**, *137*, 205–208. [CrossRef]
8. Chen, C.H.; Shih, W.C.; Chien, C.Y.; Hsu, C.H.; Wu, Y.H.; Lai, C.H. A promising sputtering route for one-step fabrication of chalcopyrite phase Cu(In,Ga)Se_2 absorbers without extra se supply. *Sol. Energy Mater. Sol. Cells* **2012**, *103*, 25–29. [CrossRef]
9. Ouyang, L.; Zhuang, D.; Zhao, M.; Gong, Q.; Guo, L.; Sun, R.; Zhang, L. Cu(In,Ga)Se_2 solar cells fabricated by sputtering from copper-poor and selenium-rich ceramic target with selenium-free post treatment. *Mater. Lett.* **2016**, *184*, 69–72. [CrossRef]
10. Zhang, L.; Zhang, W.; Liu, J.; Ma, Q.; Ma, X.; Wu, R.; Song, H.; Song, D.; Zhang, L.; Zhang, H. Solvothermal synthesis of chalcopyrite $CuIn_{0.7}Ga_{0.3}Se_2$ nanoparticles and the studies on reaction mechanism and structure defects. *Mater. Chem. Phys.* **2014**, *147*, 390–394. [CrossRef]
11. Hsu, W.-H.; Hsiang, H.-I.; Chen, M.-H.; Chen, C.-C. Cuinse$_2$ formation from CuSe/In_2Se_3 and Cu_2Se/In_2Se_3 powders: Reaction kinetics and mechanisms. *J. Am. Ceram. Soc.* **2014**, *97*, 2439–2446. [CrossRef]
12. Hsu, W.-H.; Hsiang, H.-I.; Chang, Y.-L.; Ray, D.-T.; Yen, F.-S. Formation mechanisms of Cu($In_{0.7}Ga_{0.3}$)Se_2 nanocrystallites synthesized using hot-injection and heating-up processes. *J. Am. Ceram. Soc.* **2011**, *94*, 3030–3034. [CrossRef]
13. Li, X.; Zhao, M.; Zhuang, D.; Cao, M.; Ouyang, L.; Guo, L.; Gao, Z.; Sun, R. Influences of na on sintering of Cu(In, Ga)Se_2 quaternary ceramic targets. *J. Alloys Compd.* **2015**, *636*, 335–340. [CrossRef]
14. Zhang, W.J.; Wang, T.M.; Wu, X.W.; Zhong, L.Z.; Min, C. Optimized design for preparing nanocrystalline ITO powder. *Rare Met. Mater. Eng.* **2005**, *34*, 1352–1356.
15. Feng, J.; Huang, X.; Chen, W.; Wu, J.; Lin, H.; Cheng, Q.; Yun, D.; Zhang, F. Fabrication and characterization of Cu_2ZnSnS_4 thin films for photovoltaic application by low-cost single target sputtering process. *Vacuum* **2016**, *126*, 84–90. [CrossRef]
16. Li, X.; Zhao, M.; Zhuang, D.; Cao, M.; Ouyang, L.; Guo, L.; Sun, R.; Gao, Z. Fabrication of Se-rich Cu($In_{1-x}Ga_x$)Se_2 quaternary ceramic target. *Vacuum* **2015**, *119*, 15–18. [CrossRef]
17. Ning, Z.; Da-Ming, Z.; Gong, Z. An investigation on preparation of CIGS targets by sintering process. *Mater. Sci. Eng. B Adv. Funct. Solid State Mater.* **2010**, *166*, 34–40. [CrossRef]
18. Hsu, W.-H.; Hsiang, H.-I.; Yen, F.-C.; Shei, S.-C. Two-step sintering of nanocrystalline Cu($In_{0.7}Ga_{0.3}$)Se_2. *Ceram. Int.* **2015**, *41*, 547–553. [CrossRef]
19. Lakshmi, M.; Bindu, K.; Bini, S.; Vijayakumar, K.P.; Kartha, C.S.; Abe, T.; Kashiwaba, Y. Reversible $Cu_{2-x}Se \leftrightarrow Cu_3Se_2$ phase transformation in copper selenide thin films prepared by chemical bath deposition. *Thin Solid Films* **2001**, *386*, 127–132. [CrossRef]
20. Yang, L.; Chen, Z.-G.; Han, G.; Hong, M.; Zou, Y.; Zou, J. High-performance thermoelectric Cu_2Se nanoplates through nanostructure engineering. *Nano Energy* **2015**, *16*, 367–374. [CrossRef]
21. Kim, H.; Ballikaya, S.; Chi, H.; Ahn, J.P.; Ahn, K.; Uher, C.; Kaviany, M. Ultralow thermal conductivity of β-Cu_2Se by atomic fluidity and structure distortion. *Acta Mater.* **2015**, *86*, 247–253. [CrossRef]
22. Chalapathi, U.; Poornaprakash, B.; Park, S.-H. Growth and properties of co-evaporated Cu_2SnS_3 thin films for solar cell applications. *Vacuum* **2016**, *131*, 22–27. [CrossRef]
23. Sheu, H.-H.; Hsu, Y.-T.; Jian, S.-Y.; Liang, S.-C. The effect of cu concentration in the photovoltaic efficiency of CIGS solar cells prepared by co-evaporation technique. *Vacuum* **2016**, *131*, 278–284. [CrossRef]
24. Mohan, C.R.; Sathya, R.; Nithiananthi, P.; Jayakumar, K. Ultrasonic velocimetry studies on different salts of chitosan: Effect of ion size. *Int. J. Biol. Macromol.* **2017**, *104*, 1596–1603. [CrossRef] [PubMed]
25. Nagapure, D.R.; Patil, R.M.; Mary, G.S.; Chandra, G.H.; Sunil, M.A.; Subbaiah, Y.P.V.; Gupta, M.; Rao, R.P. Effect of selenium incorporation at precursor stage on growth and properties of $Cu_2ZnSnSe_4$ thin films. *Vacuum* **2017**, *144*, 43–52. [CrossRef]